Intermediate progenitors are increased by lengthening of the cell cycle through calcium signaling and p53 expression in human neural progenitors

Elisa García-García, María José Pino-Barrio, Laura López-Medina, and Alberto Martínez-Serrano
Department of Molecular Biology and Center of Molecular Biology "Severo Ochoa," Universidad Autónoma de Madrid, Consejo Superior de Investigaciones Científicas, Cantoblanco, 28049 Madrid, Spain

ABSTRACT **During development, neurons can be generated directly from a multipotent progenitor or indirectly through an intermediate progenitor (IP). This last mode of division amplifies the progeny of neurons. The mechanisms governing the generation and behavior of IPs are not well understood. In this work, we demonstrate that the lengthening of the cell cycle enhances the generation of neurons in a human neural progenitor cell system in vitro and also the generation and expansion of IPs. These IPs are insulinoma-associated 1 (*Insm1*)$^+$/BTG family member 2 (*Btg2*)$^-$, which suggests an increase in a self-amplifying IP population. Later the cultures express neurogenin 2 (*Ngn2*) and become neurogenic. The signaling responsible for this cell cycle modulation is investigated. It is found that the release of calcium from the endoplasmic reticulum to the cytosol in response to B cell lymphoma-extra large overexpression or ATP addition lengths the cell cycle and increases the number of IPs and, in turn, the final neuron outcome. Moreover, data suggest that the p53–p21 pathway is responsible for the changes in cell cycle. In agreement with this, increased p53 levels are necessary for a calcium-induced increase in neurons. Our findings contribute to understand how calcium signaling can modulate cell cycle length during neurogenesis.**

Monitoring Editor
Kunxin Luo
University of California, Berkeley

Received: Jun 16, 2011
Revised: Dec 19, 2011
Accepted: Jan 30, 2012

INTRODUCTION

Understanding neuron generation from their precursors is of interest from a developmental point of view and also for improving drug screening, diagnostic, and therapeutic strategies. The whole CNS starts developing from just a layer of neural progenitor/stem cells (NPCs) that expand through rounds of symmetric proliferative divisions. Later they start to differentiate into the diverse cell types of the CNS (Gotz and Huttner, 2005). The first progeny to appear is the neuron population (Qian *et al.*, 2000). NPCs achieve neurogenesis by changing their symmetric, self-renewing division into 1) self-consuming neurogenic division, producing two neurons, or 2) asymmetric division, in which one cell remains an NPC while its sister becomes either a neuron, or 3) a mitotic intermediate progenitor (IP). Understanding the decision taken by an NPC between differentiating directly into a neuron or through an IP is of relevance because the amplification of neuronal precursors leads to an increase in the final neural outcome and defines the final size and structure of the CNS (Miyata *et al.*, 2004; Huttner and Kosodo, 2005; Farkas and Huttner, 2008; Noctor *et al.*, 2008; Zhong and Chia, 2008). Indeed, mutations in genes regulating the division modes of NPCs during development produce severe brain malformations (Bond and Woods, 2006; Fish *et al.*, 2008). Moreover, knowledge of the mechanisms guiding the generation of IPs is a key to explaining the differences between the cortex size in gyrencephalic and lissencephalic brains in terms of evolution (Kriegstein *et al.*, 2006). In the present study, we investigated the mechanisms involved in the generation of IPs as governed by

This article was published online ahead of print in MBoC in Press (http://www.molbiolcell.org/cgi/doi/10.1091/mbc.E11-06-0524) on February 9, 2012.

Address correspondence to: Elisa García-García (egarcia@cbm.uam.es).

Abbreviations used: BAPTA-AM, 1,2-bis(*o*-aminophenoxy)ethane-*N*,*N*,*N*′,*N*′-tetraacetic acid tetra(acetoxymethyl); Bcl-XL, B cell lymphoma-extra large; BrdU, 5-bromo-2′-deoxyuridine; Btg2, BTG family member 2; EdU, 5-ethynyl-2′-deoxyuridine; EGF, epidermal growth factor; EGTA, ethylene glycol tetraacetic acid; ER, endoplasmic reticulum; FGF2, basic fibroblast growth factor; Insm1, insulinoma-associated 1; Ins3P, inositol trisphosphate or inositol 1,4,5-trisphosphate; IP, intermediate progenitor; Ngn2, neurogenin 2; NPCs, neural progenitor cells; Pax6, paired box 6; PBS, phosphate-buffered saline; shRNA, small (short) hairpin RNA; Sox2, (sex determining region Y)-box 2.

the balance between proliferation and differentiation in human NPCs (hNPCs).

Many cues—external and internal—regulate the balance between proliferation and differentiation. One is the rate of progression through the cell cycle (Dehay and Kennedy, 2007; Doe, 2008). Correlation has been established between the length of cell cycle and the differentiation potential of progenitors (Salomoni and Calegari, 2010). Experiments on forced lengthening of the cell cycle in rodents promoted an increase in neurons, demonstrating the causal relationship between cell cycle length and neurogenesis (Calegari and Huttner, 2003). On the other hand, recent work described how the IPs have a longer cell cycle than noncommitted progenitors in the mouse cerebral cortex, probably due to its more differentiated state. However, it is an open issue whether lengthening the cell cycle promotes the IP fate from NPCs (Arai *et al.*, 2011.).

During recent years, cell cycle inhibitors have been shown to play key roles in regulating proliferation versus differentiation choice during neurogenesis, and many external cues have been reported to modulate them (Ohnuma *et al.*, 2001; Besson *et al.*, 2008; Joseph and Hermanson, 2010). However, work based on clonal neural progenitor cultures concluded that neurogenic timing is also defined by cell-intrinsic determinants (Qian *et al.*, 2000; Shen *et al.*, 2006). The precise nature and mechanism of action of these intrinsic determinants are not understood.

Another regulator of final brain size, tightly linked to the cell cycle, is programmed cell death, acting not merely as a clearing process of unwanted cells, but also as a necessary event during development (Garrido and Kroemer, 2004). In this way, animals lacking some of the proapoptotic members, such as Bak or Bax, show brain overgrowth (Lindsten *et al.*, 2003). To add more complexity, an increasing number of studies have showed that cell death of key proteins, such as caspase-3, also play a role in developmental process per se, not directly related to cell death (Kuranaga and Miura, 2007; Kuranaga, 2011). Key proteins important for the decision of cell survival versus death are the members of the Bcl-2 family, with proapoptotic members such as Bax and Bak, or BH3-only proteins and antiapoptotic members like Bcl-2, B cell lymphoma-extra large (Bcl-XL), and Mcl-1 (Youle and Strasser, 2008). In recent years, we and others have demonstrated that Bcl-XL has a significant effect on the differentiation of murine and human NPCs in vitro and in vivo, promoting the generation of more neurons—specifically those with a dopaminergic phenotype (Liste *et al.*, 2004, 2007; Shim *et al.*, 2004; Chang *et al.*, 2007).

Our previous work demonstrated that Bcl-XL increases the amount of neurons generated from human NPCs, using the hNS1 cell differentiation system as a model of in vitro and in vivo neurogenesis. This increase was not due to counteracting cell death but to enhancing the neuronal progenitor population (Liste *et al.*, 2007; Courtois *et al.*, 2010). On the basis of this finding, in the present work we further study the cellular and molecular mechanisms by which Bcl-XL promotes neurogenesis as a model to determine novel mechanisms that govern the generation and expansion of IPs.

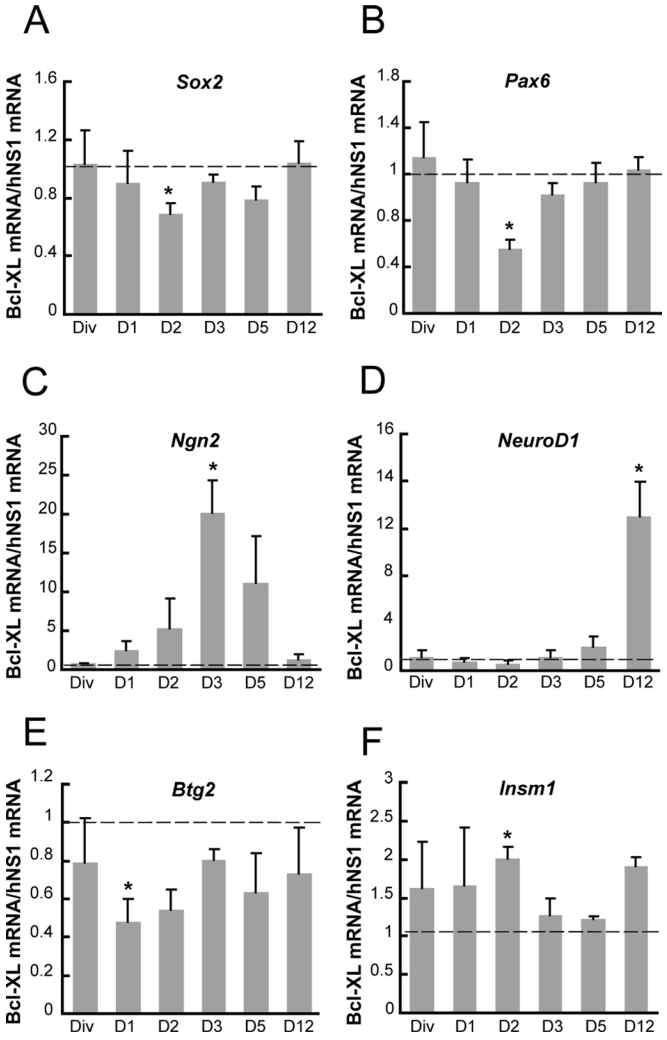

FIGURE 1: Increased Bcl-XL enlarges the neuronal committed progenitor population. mRNA levels of key developmental transcription factors present in neural progenitor (A) *Sox2* and (B) *Pax6*, neuronal lineage (C) *Ngn2* and (D) *NeuroD1*, and intermediate progenitors (E) *Btg2* and (F) *Inms1* were measured on the indicated days by quantitative real-time PCR, relative to the mRNA levels present in hNS1 cells. GAPDH expression was used as a total normalizing mRNA. Dashed line indicates equal levels of expression between Bcl-XL and hNS1 cells. Data are means ± SEM (n = 4), and asterisk indicates a significant difference ($p < 0.05$) from the value 1 (equal expression in both cell types) by interval of confidence analysis.

RESULTS

Lengthening the cell cycle increases the number of IPs

We previously showed that an increased level of Bcl-XL protein during the differentiation of hNS1 cells enhances neuronal progenitor proliferation (Liste *et al.*, 2007). Thus, before studying in depth this model of neuronal progenitor generation, we asked about the molecular identity of the enlarged progenitor population, according to different transcription factors expressed in different cell populations during development (Guillemot, 2007). To this end, we compared a stable subclone with forced expression of Bcl-XL to the parental hNS1 control cells. First, we observed that mRNA levels of transcription factors present in uncommitted progenitors—(sex determining region Y)-box 2 (*Sox2*) and paired box 6 (*Pax6*)—were reduced in Bcl-XL cells during day 2 of differentiation (Figure 1, A and B). Second, the bHLH neurogenin 2 (*Ngn2*) transcription factor, which induces neuronal choice from progenitors, was transiently increased on day 3 of differentiation in Bcl-XL cells in comparison to control hNS1 cells (Figure 1C). Third, *NeuroD1*, a bHLH transcription factor involved in terminal neuronal differentiation, was increased at later days of differentiation in Bcl-XL cells (Figure 1D). Finally, the marker for neurogenic progenitor BTG family member 2 (*Btg2*; human homologue of mouse *Tis21*) was reduced during day 2 (Figure 1E), but insulinoma-associated 1 (*Insm1*), a marker for proliferative IP, was

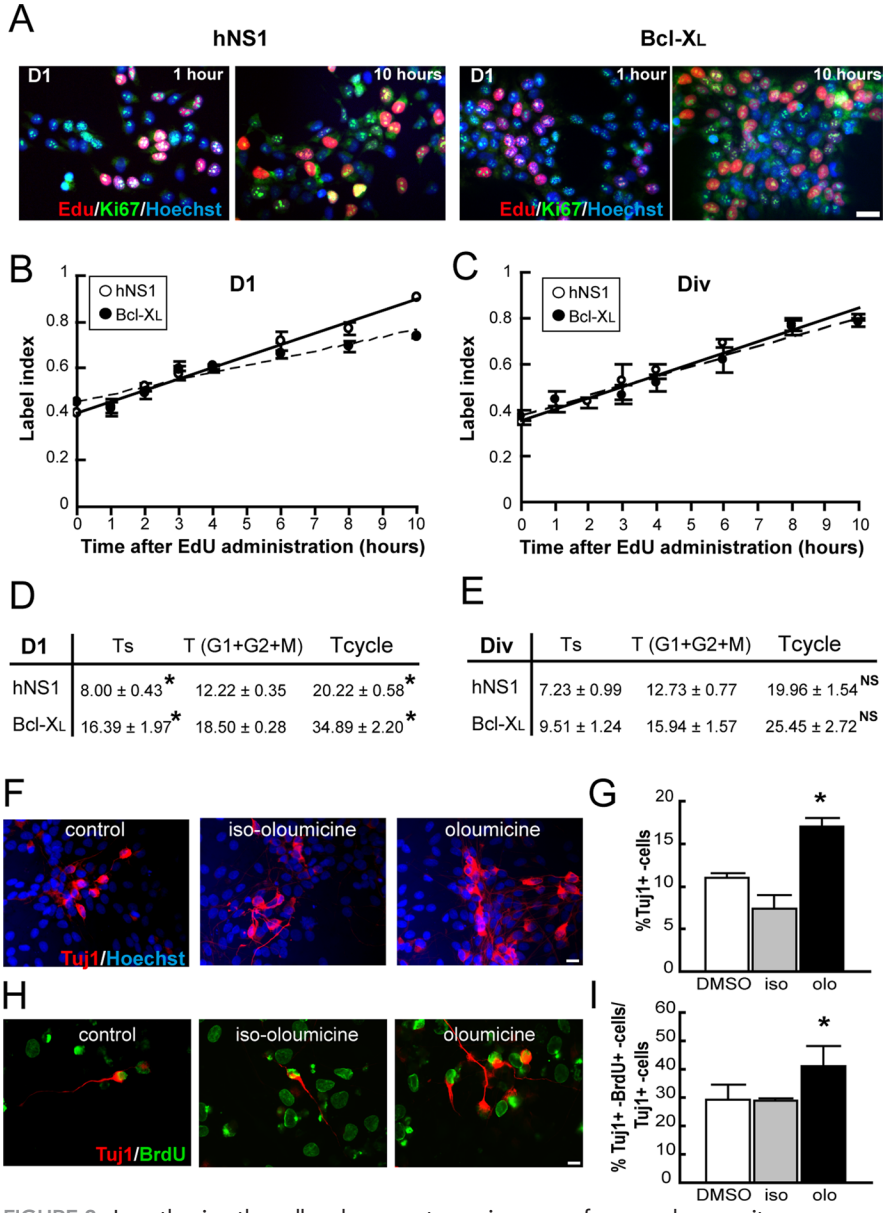

D1	Ts	T (G1+G2+M)	Tcycle
hNS1	8.00 ± 0.43*	12.22 ± 0.35	20.22 ± 0.58*
Bcl-XL	16.39 ± 1.97*	18.50 ± 0.28	34.89 ± 2.20*

Div	Ts	T (G1+G2+M)	Tcycle
hNS1	7.23 ± 0.99	12.73 ± 0.77	19.96 ± 1.54NS
Bcl-XL	9.51 ± 1.24	15.94 ± 1.57	25.45 ± 2.72NS

FIGURE 2: Lengthening the cell cycle promotes an increase of neuronal progenitor population in differentiating hNS1 cells. EdU 10 μM was administrated to Bcl-XL and control hNS1 cells at 24 h after growth factor withdrawal (D1) or in the presence of growth factors (Div; time 0), and cultures were fixed at different times. (A) Representative pictures of EdU detection (red) combined with immunostaining for Ki67 (green) and counterstained with Hoechst (blue) on day 1. Scale bar, 25 μm. (B, C) Graphs show the EdU labeling index (EdU$^+$ cells in the Ki67$^+$ pool). Data represents means ± SEM (n = 4), and lines show the best fits (r^2 = 0.980897 and 0.9173 for control hNS1 [solid line] and Bcl-XL cells [dashed line], respectively, on D1 and r^2 = 0.9916 and 0.9191, respectively, on Div). (D, E) Summary of the obtained data. The cell cycle length (Tcycle) is the sum of the duration of the S phase (Ts) plus the duration of G1 + G2 + M phases (T) per experiment. Data are means ± SEM (n = 4), and the asterisk indicates a significant difference between cell types ($p < 0.01$, Student's *t* test). There is a statistically significant increase of the S-phase and total cell cycle length in Bcl-XL cells when compared with control hNS1 cells on day 1 of differentiation. (F) Oloumicine (15 μM) and its inert form iso-oloumicine (15 μM) were applied to hNS1 cells at day 1 of differentiation for 24 h, and cells were fixed on day 8 of differentiation and stained for Tuj1 (red) and Hoechst (blue). Scale bar, 25 μm. (H) Oloumicine (15 μM) and iso-oloumicine (15 μM) were added to hNS1 cultures on day 1 for 24 h; on day 2, BrdU (1 μM) was added for another 24 h, then cells were let to differentiate until day 8 and stained for Tuj1 cells (red) and BrdU (green). Scale bar, 25 μm. (G, I) There was a higher number of Tuj1$^+$ cells and double BrdU$^+$–Tuj1$^+$ cells on day 8 of differentiation only in oloumicine-treated cultures. Data are means ± SEM (n = 4), and the asterisk indicates a significant difference versus the other groups ($p < 0.05$, one-way analysis of variance (ANOVA), followed by a Fisher test).

increased in Bcl-XL cells (Figure 1F). All of these data are consistent with an increase in the number of proliferative IPs (*Insm1*$^+$, *Btg2*$^-$) on day 2 at the expense of uncommitted progenitors (*Pax6*$^+$, *Sox2*$^+$). Then these IPs become neurogenic (*Ngn2*$^+$) on day 3, and later they render terminally differentiated neurons (*NeuroD1*$^+$).

Bcl-XL has been involved in the control of cell cycle (Janumyan *et al.*, 2008), and cell cycle duration is central in the decision of differentiation versus proliferation (Arai *et al.* 2011). Thus we asked whether the increase in IPs and neurogenesis observed in this model correlates with an increase in the length of cell cycle. To this end, we measured the cell cycle length in a Bcl-XL gain-of-function situation. According to the foregoing data and with the conditions of the mathematical model used (see *Materials and Methods*), the experiment was run on day 1 of differentiation, when fate decisions are being taken in a homogeneous, dividing, Ki67$^+$ marker population (Figure 2A). As Figure 2, B and D, illustrates, Bcl-XL cells had longer cell cycle than did hNS1 control cells on day 1 of differentiation. In addition, Bcl-XL cultures presented an increase in S-phase length. Because this set of experiments was run with a stable, overexpressing Bcl-XL clone, we also analyzed the length of the cell cycle under proliferation conditions to test whether cell cycle lengthening by Bcl-XL occurs only during differentiation (Figure 2C, DIV conditions; Villa *et al.*, 2000). Under these conditions, Bcl-XL did not induce a lengthening of cell cycle or of the S phase (Figure 2E).

It also was shown that lengthening of the cell cycle can increase the number of neurons in mouse in vitro and in vivo (Salomoni and Calegari, 2010). We then asked whether the same phenomenon also applied to a human model system such as the one used here. To this aim, we applied oloumicine on day 1 of differentiation for 24 h; this is a cdk inhibitor that at low concentration slows the progression through G1 phase (Calegari and Huttner, 2003). Then we allowed the cells to differentiate and quantified the number of neurons. By doing this, we could observe that the oloumicine-induced lengthening of the cell cycle on day 1 produces an increase in the number of Tuj1$^+$ cells after 8 d of differentiation (Figure 2, F and G). In addition, we repeated the experiment in Bcl-XL cells and observed no increment in the number of neurons after olocumicine treatment (Supplemental Figure S1). We next asked whether the lengthening of the cell cycle causally contributes to an increase of IP population. To this end, we added oloumicine as previously described and monitored the progenitors by pulsing hNS1 cells with 5-bromo-2′-deoxyuridine (BrdU) on day 2 of the differentiation for 24 h. Then cells were allowed to differentiate until day 8, and the number of

double Tuj1+/BrdU+ cells was quantified relative to the total number of neurons (Figure 2H). The cultures grown in the presence of oloumicine for 24 h had a higher number of double-stained neurons, indicating a larger progenitor population on days 2–3 of differentiation (Figure 2I).

Taking these data together, we conclude that elevated levels of Bcl-XL lead to an increased IP population, identified by *Insm1* and *Ngn2*, and this effect is achieved by cell cycle lengthening.

Bcl-XL enhances neurogenesis by modulating the p53–p21 pathway

The next aim was to determine which cell cycle regulator is responsible for the lengthening of the cell cycle when Bcl-XL levels are increased. We focused on the Kip/Cip1 family—p57, p27 and p21—which are known to play key roles in cell cycle regulation during CNS development (Joseph and Hermanson, 2010). First, we analyzed their nuclear protein levels during the first days of differentiation, especially on day 1. We observed that low expression of p57 did not change during these days; p27 increased and p21 decreased as differentiation progressed (Figure 3A). There were no differences in p57 levels between Bcl-XL and control hNS1 cells. On the other hand, Bcl-XL cells had lower p27 levels than control cells (Figure 3, A and B). We then focused on p27 and quantified its expression at longer time points. We observed that Bcl-XL cells contained lower amounts of p27 during days 3 and 4, but its expression became similar to that of control cells afterward (Figure 3, B and C). Because the cell cycle inhibitor p21 was increased in Bcl-XL cells during day 1 of differentiation (Figure 3A), we studied the expression of a known regulator of p21 activity, p53 (Boulaire *et al.*, 2000). We observed that Bcl-XL cells had higher levels of p53 protein than did control hNS1 cells during the initial days of differentiation (Figure 3, D and E). In addition, 30.11 ± 2.2% of the total Bcl-XL cells were p53+ as compared with 18.78 ± 1.72% p53+ cells in control hNS1 cells on day 1 of differentiation (Figure 4A). Moreover, the intensity for p53 immunoreactivity in Bcl-XL–overexpressing cells was higher than in control cells (Figure 4, A and B).

To determine that the results observed were specific to Bcl-XL and not just the result of a long-term exposure of the cultures to an antiapoptotic protein, first we demonstrated that a transient expression of Bcl-XL in hNS1 cells on day 1 (scheme in Figure 4C) produces a threefold increase in the levels of p53 (Figure 4D) and second we down-regulated the transgene Bcl-XL with specific small hairpin RNA (shRNA; Supplemental Figure S2A). This induced a recovery of hNS1 phenotype in terms of the number of p53+ cells (Supplemental Figure S2, B and C) and Tuj1+ cells (Supplemental Figure S2, D and E). As a result, we propose that the increase in neurons observed after the forced expression of Bcl-XL is due to an increase of p53 protein. To verify this hypothesis, we infected Bcl-XL cells with lentiviral vectors coding for interfering shRNA to decrease p53 levels and also with control vectors (infection efficiency was ~95% for all vectors; Supplemental Figure S3). After 8 d of differentiation, the cultures infected with shRNAs 14 and 55 contained ~12% fewer neurons than the cultures infected with an empty vector (turbo green fluorescent protein [tGFP]; Figure 4, E and F). Therefore we demonstrated that the increase in the number of neurons occurring after the forced expression of Bcl-XL is mediated by an increased level of p53 during the first days of differentiation.

Increased cytosolic calcium lengthens cell cycle and promotes IP generation and neurogenesis

Next we asked how Bcl-XL increases the levels of p53. Our first approach was to check whether both proteins could colocalize by

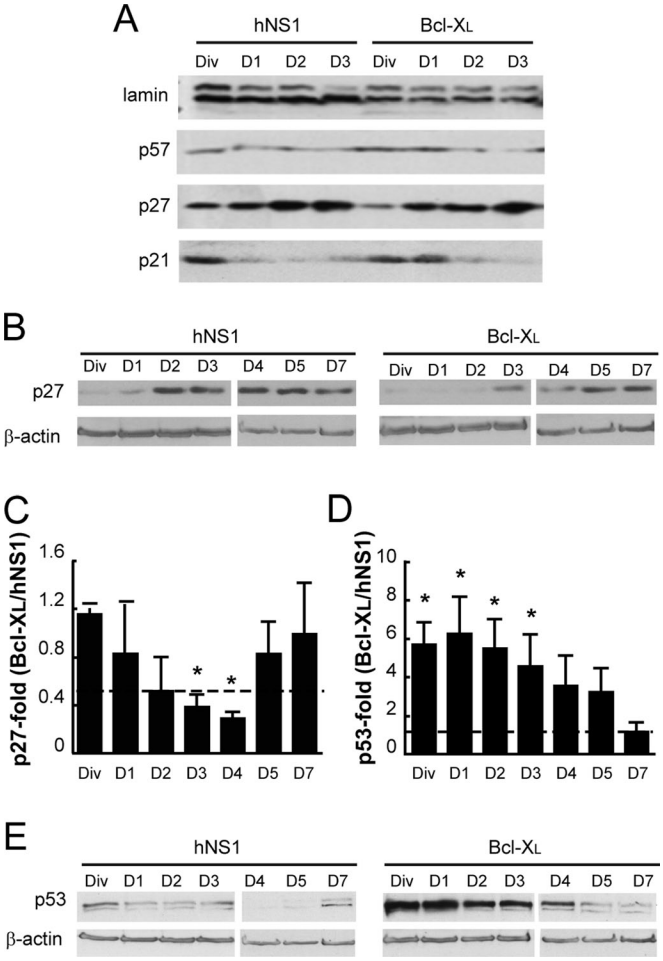

FIGURE 3: The p53–p21 pathway is enhanced by Bcl-XL expression. (A) Western blot of nuclear lysates isolated from Bcl-XL and control hNS1 cells on the first days of differentiation. The blotted membranes were probed against antibodies for Cip/Kip1 family members; p21 was the only member that was increased in Bcl-XL when compared with control hNS1 cells. (B) Total cell lysates were collected from Bcl-XL and hNS1 cells on the indicated days and then blotted and probed against p27. (C) Densitometry of p27 data normalized to β-actin plotted as the ratio between Bcl-XL and control hNS1 cells for every analyzed day. Dashed line shows equal p27 level (ratio, 1). Lower p27 ratios in Bcl-XL than hNS1 cells on days 3 and 4 indicate a higher progenitor population. (D) Densitometry shows that p53 protein is augmented during the first days of differentiation. Data are means ± SEM (n = 5). The asterisk indicates significant difference ($p < 0.05$) from a value of 1 (equal values) by interval of confidence analysis. (E) Representative image of a Western blot in which total cell lysates were blotted and analyzed for p53.

determining their compartmentalization, since an interaction between them was reported (Hagn *et al.*, 2010). As Figure 4G shows, an interaction between them is unlikely because the pattern of Bcl-XL expression resembles mitochondrial staining, whereas p53 is present in the nucleus. Therefore we hypothesized that there must be a signaling pathway that works as an intermediary between Bcl-XL and the regulation of the cell cycle by p53. To answer this, we studied calcium signaling as a possible link, due to the importance of calcium in cell cycle regulation and the already known effects of Bcl-XL on Ins3P receptor (White *et al.*, 2005; Lipskaia *et al.*, 2009). First we found a transient increase in cytosolic calcium levels in Bcl-XL cells on day 1 of differentiation, which was absent in the presence

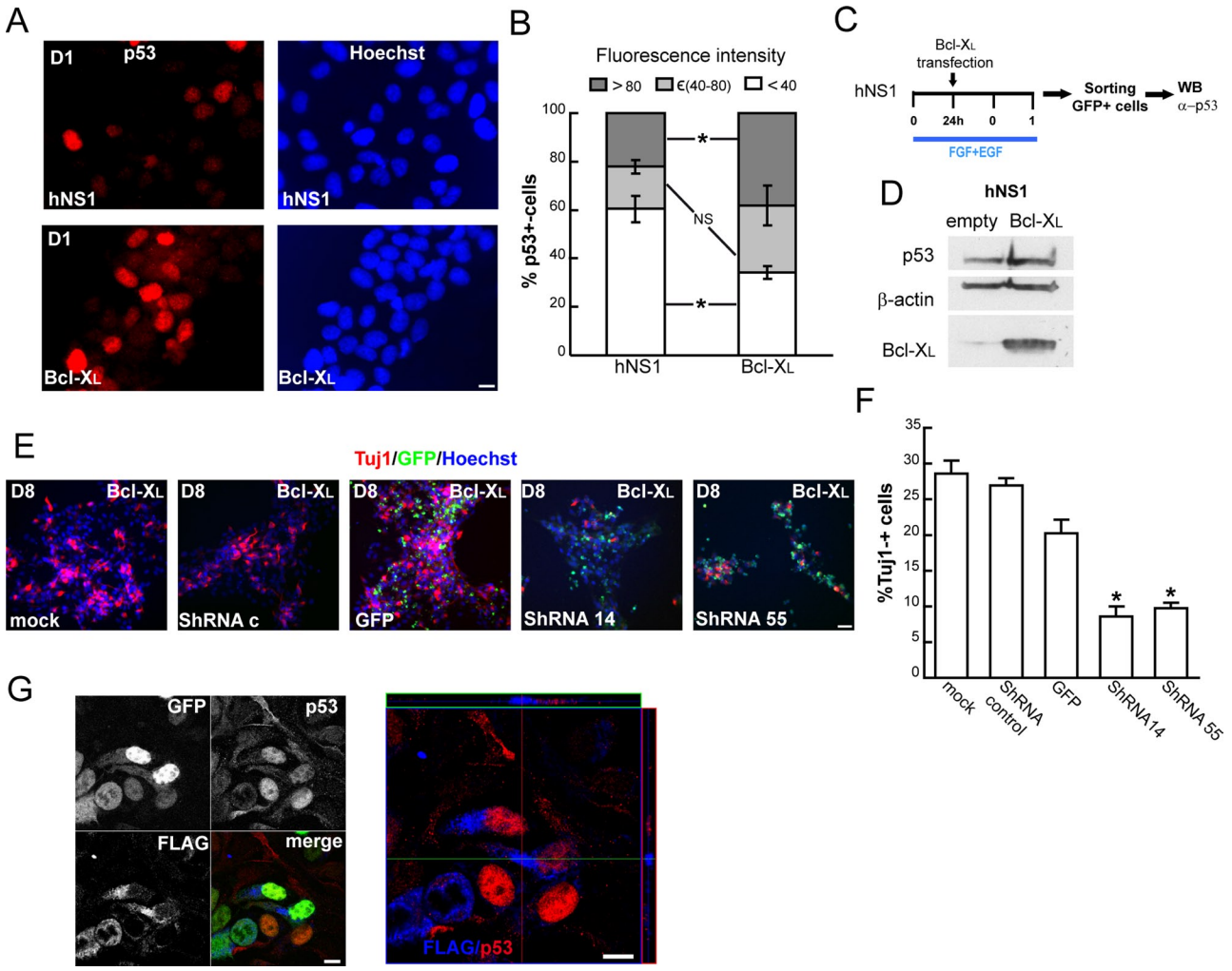

FIGURE 4: Bcl-XL increases the neuron population through p53. (A) Representative images of p53 IF taken on day 1 of differentiation from fixed Bcl-XL and control hNS1 cultures. Scale bar, 10 μm. (B) Graphs representing the relative fluorescence levels among $p53^+$ cells split into three intervals: low fluorescence, below a threshold of 40 arbitrary units (U); medium, between 40 and 80 U; and high, greater than a threshold of 80 U. The number of $p53^+$ cells analyzed was >50 in control hNS1 and >120 cells in Bcl-XL in three independent experiments. The asterisk indicates a significant difference in low- and high-fluorescence $p53^+$ cells between Bcl-XL and control hNS1 cells. (n = 3, two-way ANOVA, $p < 0.01$ for the interaction, followed by a Fisher post hoc analysis; NS, nonsignificant difference). (C) hNS1 or hNPCs (nonimmortalized) were transfected with pCAGGs-Bcl-XL-IRES-GFP or pCAGGs-empty-IRES-GFP as a control in the presence of growth factors (division conditions); 24 h later, cells were allowed to differentiate. At 48 h after transfection, cells were sorted by GFP fluorescence with a purity of ~95% in all of the cases. (D) Representative Western blot; protein from 75,000 cells was blotted and membranes probed against p53, β-actin, and Bcl-XL (three independent experiments). (E) Bcl-XL–overexpressing cells were infected with a lentiviral vector transducing the indicated shRNAs against p53 or with control vectors. Cultures were fixed on day 8 of differentiation and stained for Tuj1 (red) and Hoechst (blue); GFP^+ cells are shown in green. Scale bar, 50 μm. (F) $Tuj1^+$ cells were quantified on day 8 of differentiation from infected cultures. Data represent means ± SEM (n = 4). The asterisk indicates significant difference ($p < 0.05$, one-way ANOVA followed by a Tukey test). The number of $Tuj1^+$ cells generated by Bcl-XL cultures is reduced in p53 shRNA–transduced cells. (G) Confocal images taken from hNS1 cells transfected with pCAGGs-FLAG:Bcl-XL-IRES-GFP and stained for FLAG (blue) and p53 (red). Scale bar, 10 μm. Note that FLAG and p53 staining do not overlap in the orthogonal projection.

of growth factors or on day 3 of differentiation (Figure 5, A–C). Second, we proved that a decrease of cytosolic calcium, induced by an efficient and nontoxic concentration of 1,2-bis(*o*-aminophenoxy) ethane-*N*,*N*,*N*′,*N*′-tetraacetic acid tetra(acetoxymethyl) (BAPTA-AM; Supplemental Figure S4) in Bcl-XL cells on day 1 of differentiation did reduce the neuron output on day 8 (Figure 5, D and E).

Thereafter, we addressed the question of whether a transient increase in cytosolic calcium on day 1 induced by means other than elevated Bcl-XL expression would have the same neurogenic effect. To this aim, we mobilized the endoplasmic reticulum (ER) calcium stores through the Ins3P pathway by addition of ATP to hNS1 cells on day 1 of differentiation (Figure 5, F–H). This ATP-induced calcium release also resulted in an increase of neurons on day 8 of differentiation (Figure 5, I and J); the same results were observed upon treatment with thapsigargin (Tg) on day 1 of differentiation (Figure 5K). To confirm that the increase in $Tuj1^+$ cells after ATP treatment

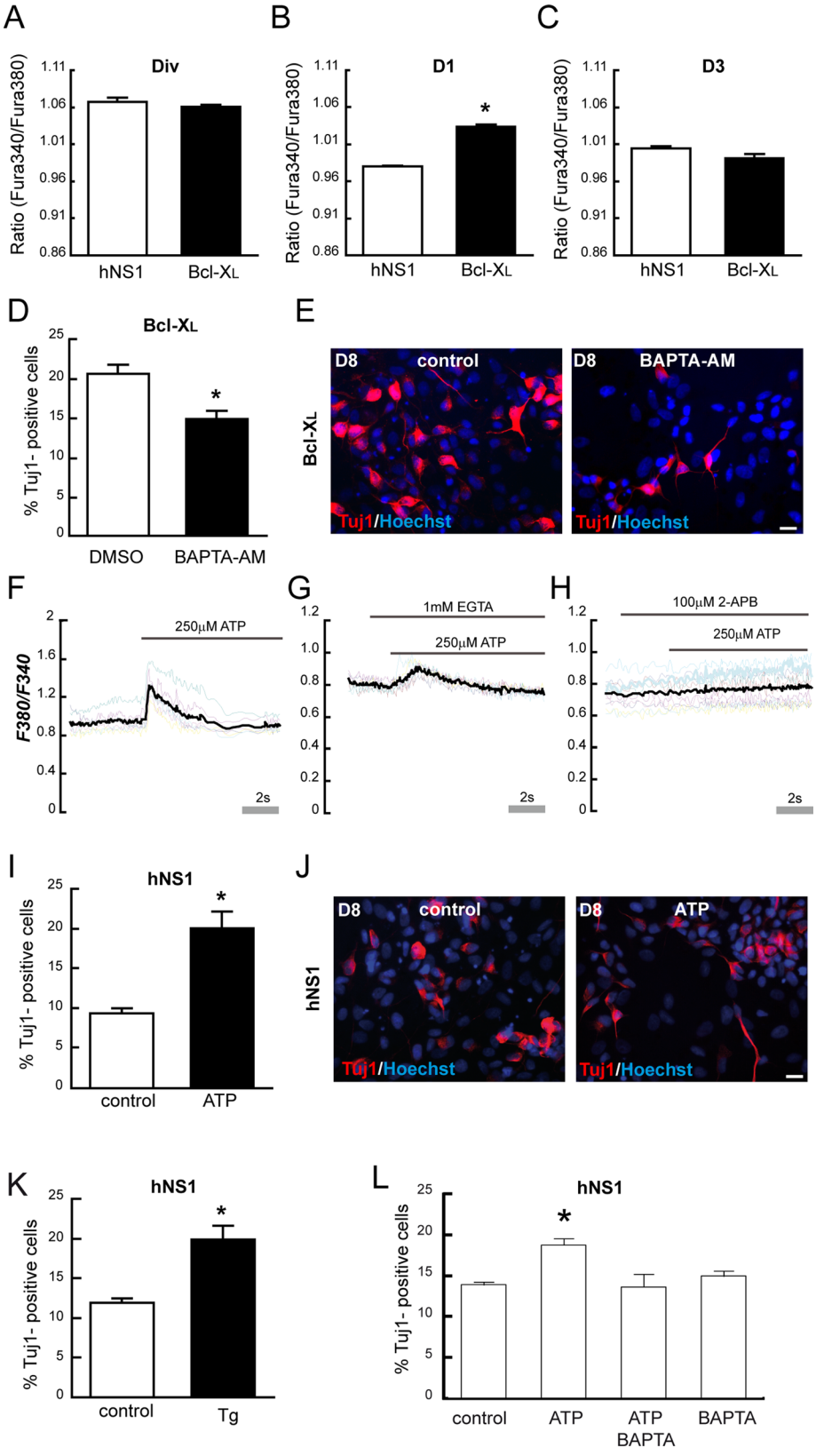

FIGURE 5: Cytosolic calcium release from the ER increases the neuron population. (A–C) Cytosolic calcium was measured using Fura-2 (ratio 340/380) on indicated days. Data represent means ± SEM (n = 3). Asterisk indicates a significant difference ($p < 0.05$, Student's *t* test, three independent experiments). There is higher cytosolic calcium in Bcl-XL cells only on day 1. (D) Quantification of Tuj1$^+$ cells in Bcl-XL–overexpression cells on day 8. Chelation of cytosolic calcium with BAPTA-AM (10 μM) on day 1 for 24 h diminishes the number of Tuj1$^+$ cells when compared with control cultures (dimethyl sulfoxide). (E) Representative IF for Tuj1 and Hoechst of cultures with or without BAPTA-AM on day 8 of differentiation. Scale bar, 25 μm. Fura-2–loaded hNS1 cells were exposed to (F) 250 μM ATP, (G) 1 mM EGTA and immediately 250 μM ATP, or (H) 2-APB (an inhibitor of Ins3P receptor) and immediately 250 μM ATP. Colored lines represent the cytosolic calcium measured by F340/F380 ratio of representative analyzed ROI; black line represents the average F340/F380 of the analyzed ROI. (I) Quantification of Tuj1$^+$ cells in hNS1 cells on day 8, previously treated with ATP (250 μM) on day 1 for 24 h. Data represent means ± SEM (n = 4). Asterisk indicates significant difference ($p < 0.05$, Student's *t* test). (J) Representative IF for Tuj1- and Hoechst-stained cultures with indicated treatments on day 8 of differentiation. Scale bar, 25 μm. (K) hNS1 cells were treated with 250 μM ATP, 10 μM BAPTA-AM, or both on day 1 of differentiation for 10 h. Then cells were allowed to differentiate until day 8; cells were fixed and stained for Tuj1 and Hoescht. The graph represents the means ± SEM. Asterisk indicates significant difference, $p < 0.01$, n = 4, one-way ANOVA followed by a Fisher post hoc test. Note that neuron increase produced by ATP treatment is abolished in the presence of BAPTA-AM (L) Tuj1$^+$ cell quantification after 1 μM Tg treatment for 24 h on day 1 of differentiation, hNS1 cells were allowed to differentiate until day 8. Data represents the means ± SEM. Asterisk indicates significant difference, $p < 0.05$, n = 4, Student's *t* test).

was caused by an increase of cytosolic calcium, we added ATP on day 1 alone or with BAPTA-AM; the presence of the calcium chelator precluded the increase of Tuj1$^+$ cells (Figure 5L).

We next checked the effects of Bcl-XL loss of function by lowering the levels of human Bcl-XL in hNS1 cells with specific shRNA (Figure 6A). We did not observe any differences in p53$^+$ cell number (Figure 6B) or cytosolic calcium levels (Figure 6C) on day 2 of differentiation or in Tuj1$^+$ cells on day 8 of differentiation (Figure 6D, white bars) between cultures infected with lentivirus transducing for effective human Bcl-XL shRNAs (shRNA00 and shRNA99 conditions) and control cultures (hNS1-mock and shRNA control conditions). The infection efficiency was ~95% of total cells. Next we stimulated with ATP hNS1 cells infected with Bcl-XL shRNA and control conditions and observed that the ATP-evoked increase of Tuj1$^+$ cells is blocked when Bcl-XL is at low levels (Figure 6, D and E). In addition, ATP treatment on day 1 in Bcl-XL cells does not enhance the number of Tuj1$^+$ cells (Supplemental Figure S5A). Taking all these data

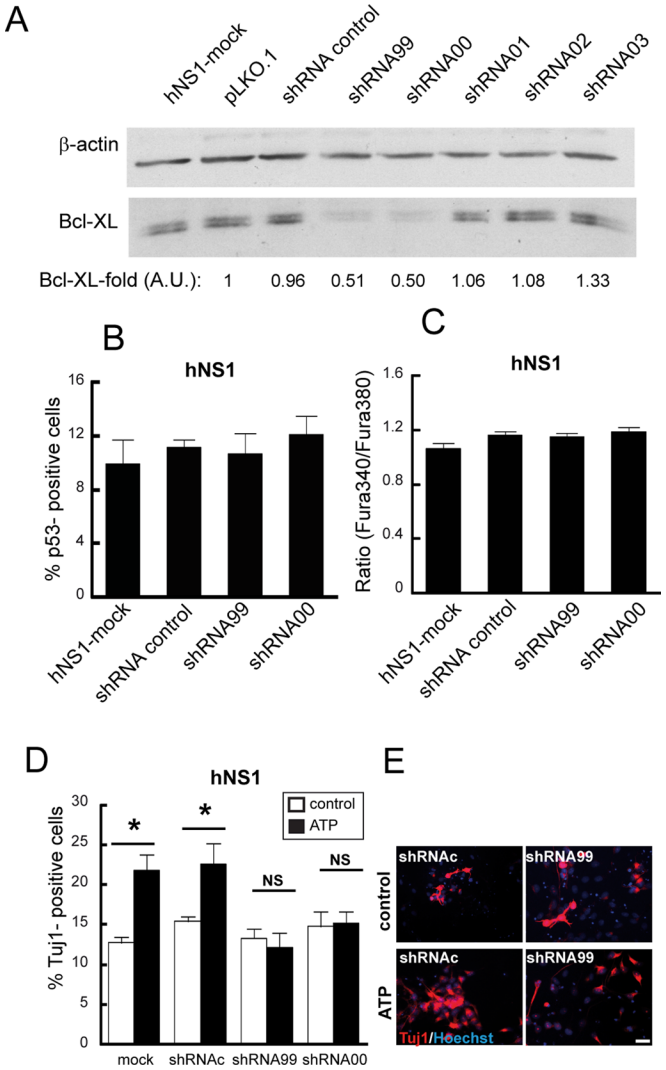

FIGURE 6: Lowering Bcl-XL produces insensitivity to ATP-evoked neurogenesis. (A) Western blot of cell lysates collected 48 h after infection. shRNA control is the scrambled shRNA control. Densitometry data are expressed as the Bcl-XL normalized by β-actin ratio of each sample between the Bcl-XL/β-actin ratio of a pLKO.1 sample. AU, arbitrary units. (B) Bcl-XL down-regulation does not decrease the number of neurons. hNS1 cells were infected with indicated lentiviral particles and allowed to differentiate for 8 d. Graph represents the percentage of Tuj1$^+$ cells. (C) Cytosolic calcium levels were measured with Fura-2 (ratio 340/380) at day 2 of differentiation after 24 h of viral infection. Data are means ± SEM. One-way ANOVA analysis indicates there is no significant difference between groups. (D). hNS1 cells were infected with indicated shRNA lentiviral particles. After 24 h of infection, cells were treated with 250 μM ATP for 10 h and fixed on day 8 of differentiation. Data represent means ± SEM. Asterisk indicates significant differences. NS, no significant differences ($p < 0.05$, two-way ANOVA followed by a Fisher post hoc test). (E) IF of ATP-treated and control cells after fixation and staining for Tuj1 and Hoescht. Scale bar. 25 μm.

together, we conclude that the effect of ATP on neurons is dependent on the levels of Bcl-XL.

We further analyzed whether the increase of neurons obtained by ATP-evoked ER calcium release correlated with an increase of cell cycle length. To evaluate this, ATP was added on day 0–1 of differentiation, and the cell cycle length of Ki67+ cells was measured after 12 h (Figure 7A). As Figure 7B shows, hNS1 cells treated with ATP have a longer cell cycle than do control cells. Moreover, S phase was also longer in ATP-treated cultures, so we propose that ATP was also enlarging the IP population. To test this, we quantified double Tuj1$^+$/BrdU$^+$ cells relative to the total number of neurons after 8 d of differentiation in cultures exposed to ATP for 24 h on day 1 and BrdU for another 24 h on day 2. In comparison to control cultures, ATP-exposed cultures present 20% more double-stained Tuj1$^+$/BrdU$^+$ neurons (Figure 7, C and D). Taking all these data together, we see that ATP and Bcl-XL, through the Ins3P pathway, mobilize calcium from ER stores and raise the cytosolic calcium levels in hNS1 cells; this causes a lengthening of the cell cycle and, in turn, an enlarged number of IPs and, as a result, of the number of generated neurons.

Increased cytosolic calcium promotes neurogenesis through the p53–p21 pathway

Next we studied whether the neurogenic effect and control of cell cycle of ATP-evoked ER calcium release was related to p53 modulation, as previously determined for Bcl-XL cells. First, we observed that p53 protein levels started to increase as soon as 8 h after ATP addition (Figure 8A). In addition, p21 protein levels peaked after 12 h of ATP exposure. The ATP effect on p53 protein level was blocked by the simultaneous incubation with BAPTA-AM (Figure 8, B–D). Next we asked whether the enlarged neuron population obtained by ATP-evoked ER calcium release was due to an increase of p53. With this aim, we performed an experiment to interfere with p53 mRNA. hNS1 cells were infected with lentivirus transducing for p53 shRNA, and the cells were then stimulated with ATP for 24 h on day 1 of differentiation and allowed to differentiate until day 8. By doing this, we observed an increase of ~5% in the neuron outcome in all of the control situations. However, after knockdown of p53 (shRNA 14 condition), ATP-evoked calcium release was not able to enhance neurogenesis (Figure 8, E and F).

Consistently, all these results demonstrate that the increase in cytosolic calcium regulates p53 levels and that the increased p53 levels are determinant for the enlarged neuron outcome.

Bcl-XL and ATP effect on IP and neuron generation of hNPCs

Finally, to rule out any immortalization-related events, we asked whether the observed effects on forced Bcl-XL expression and ATP treatment also apply when tested in a nonimmortalized hNPC in vitro system. To this end, we first transfected hNPCs (neurosphere cultures) with Bcl-XL or GFP control vectors and then quantified the number of Tuj1$^+$/GFP$^+$ cells after 8 d of transfection (Figure 9, A and B). Second, the same transfection experiment was repeated, and then the cells were let to differentiate for 24 h and GFP$^+$ cells were sorted (Figure 9C); p53 was increased in cells transfected with Bcl-XL in comparison to control cells (Figure 9D). We conclude that elevated levels of Bcl-XL increase the number of neurons and the level of p53 protein in hNPCs. Afterward, we added ATP on day 1 of differentiation to hNPCs. We observed that the number of p53$^+$ cells was increased ~15% in the presence of ATP (Figure 9, E and F) on day 2 of differentiation, as well as the number of double Tuj1$^+$/BrdU$^+$ neurons (Figure 9, G and H) and the number of Tuj1$^+$ cells (Figure 9, I and J) on day 8 of differentiation.

In conclusion, the results gathered with hNS1 cell line can be extended to a nonimmortalized, primary cell culture model of hNPCs.

DISCUSSION

In the present study we demonstrated that neurons and IPs generation from hNPC differentiation is modulated by cell cycle

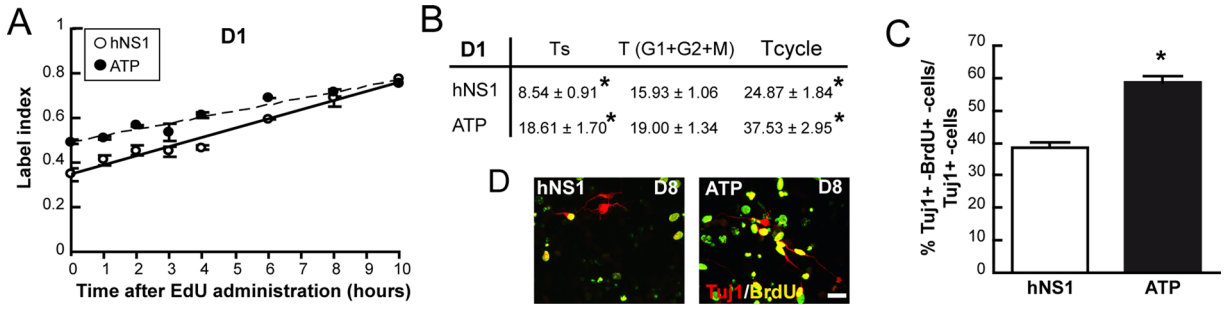

FIGURE 7: Released calcium lengthens the cell cycle and increases the number of IPs. (A) ATP 250 μM was added to the culture at 12 h after factor withdrawal, and 12 h later 10 μM EdU was administrated to hNS1 cells on the first day of differentiation (D1) and cultures were fixed at indicated times. Graphs show the EdU labeling index (EdU$^+$ cells in the Ki67$^+$ pool). Data are means ± SEM (n = 4), and lines show the best fits (r^2 = 0.9665 and 0.9412 for control hNS1 [solid line] and ATP-treated cells [dashed line], respectively, on D1). (B) Summary of the obtained data. Data are means ± SEM (n = 4) and asterisk indicates a significant difference between treatments ($p < 0.01$, Student's *t* test). (C) ATP 250 μM was added to hNS1 cultures on day 1 of differentiation for 24 h; on day 2, BrdU (1 μM) was added for another 24 h, and then cells were let to differentiate until day 8, fixed, and stained for Tuj1 (red) and BrdU (yellow). Scale bar, 25 μm. (D) Quantification of the Tuj1$^+$ cells double stained for BrdU on day 8 of differentiation. Data represent means ± SEM (n = 3), and asterisk indicates significant difference ($p < 0.05$, Student's *t* test). There was a higher number Tuj1$^+$ cells double for BrdU$^+$–Tuj1$^+$ on day 8 of differentiation after 24 h exposure of ATP on day 1 of differentiation.

length. In addition, the duration of the cell cycle is altered by calcium signaling from the ER through the control of p53 levels. Moreover, we contributed to an understanding of how the cell death–related protein Bcl-XL is able to modify the neuron outcome from hNPC differentiation by modulating the ER-released calcium.

The length of the cell cycle controls IP fate

Knowledge of how Bcl-XL increases the number of progenitors and neurons was used to understand how these two populations are generated. We determined the cell cycle length guided by the known role of Bcl-XL in the cell cycle (Zinkel *et al.*, 2006) and the importance of cell cycle duration in the balance between

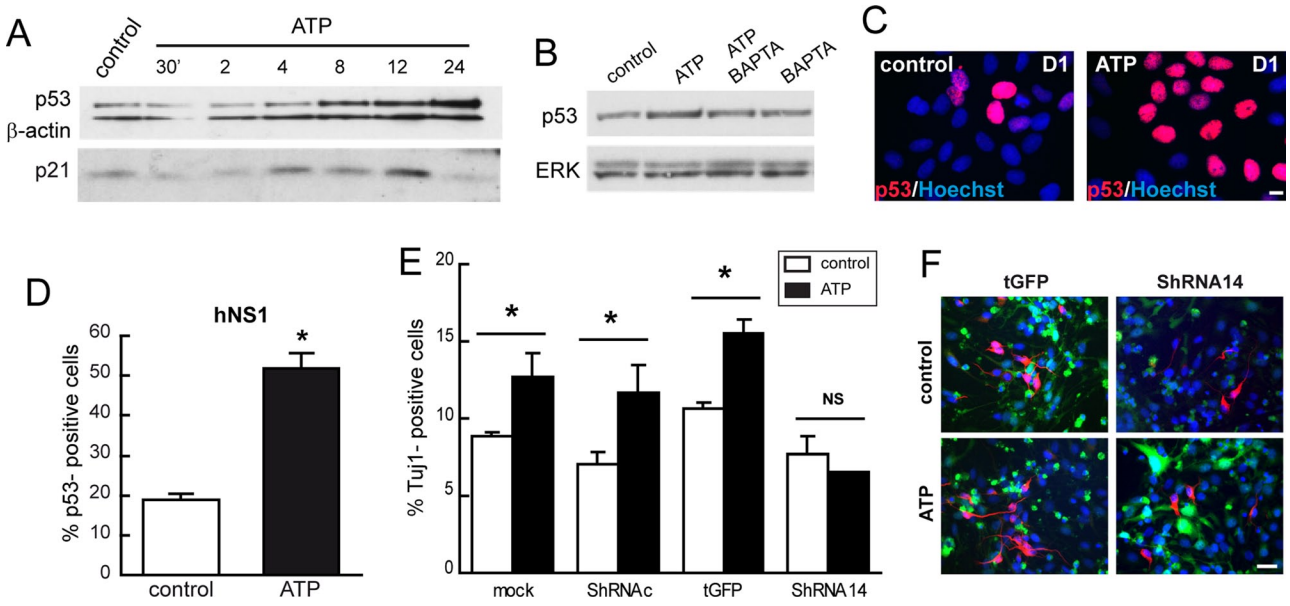

FIGURE 8: Cytosolic calcium raised by ATP increases neuron population through p53. (A) Western blot of total cell lysates from hNS1 after ATP (250 μM) addition during the indicated times. p53 starts to increase at 6–8 h after ATP exposure, and p21 peaks at 12 h after ATP exposure. (B) Western blot of total cell lysates from hNS1 cells 8 h after ATP, BAPTA-AM (10 μM), or combined ATP and BAPTA-AM (100 μM). p53 is increased after 8 h only after ATP (250 μM) exposure but not when BAPTA-AM is present. (C) Quantification of p53+ hNS1 cells treated with 250 μM ATP after 24 h of factor withdrawal during 8 h. Data are means ± SEM (n = 4), and asterisk indicates significant difference ($p < 0.05$, Student's *t* test). (D) Representative p53 immunostaining image of hNS1 control and ATP-treated cells. Scale bar, 10 μm. (E) hNS1 cells were infected with lentiviral vectors transducing the indicated shRNAs against p53 or with control vectors. After 24 h of infection, cells were stimulated with ATP for 24 h, and then cells were allowed to differentiate. Cultures were fixed on day 8 of differentiation and stained, and Tuj1$^+$ cells were quantified. Data represent means ± SEM (n = 4), and asterisk indicates significant difference ($p < 0.05$, Student's *t* test). (F) Representative images taken from hNS1 cells; Tuj1 (red), Hoechst (blue), and GFP$^+$ (green). Scale bar, 25 μm.

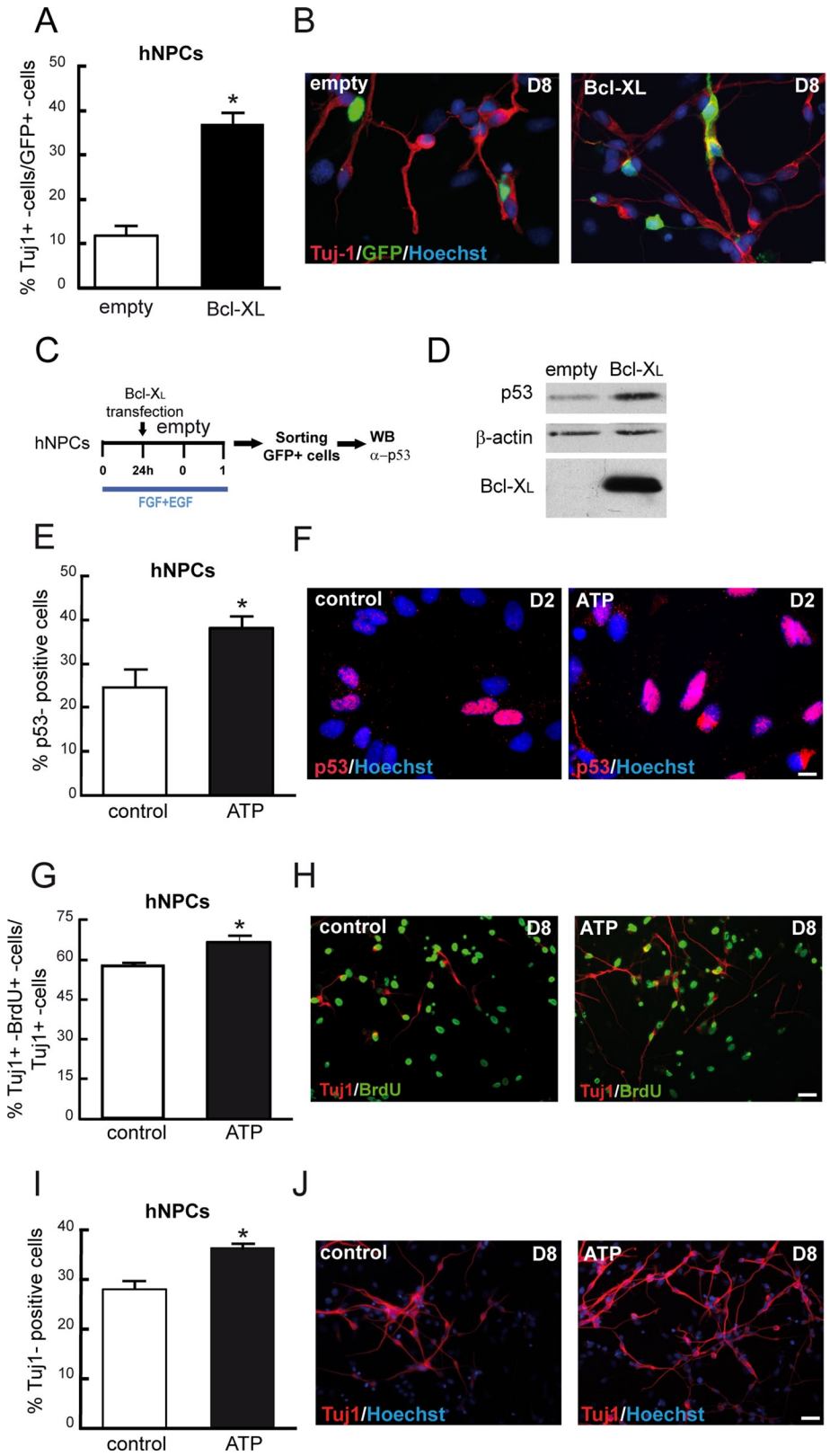

FIGURE 9: Overexpression of Bcl-XL and ATP-evoked cytosolic calcium release increase p53 levels, intermediate progenitors, and neurons in nonimmortalized hNPCs. (A) hNPCs were transfected with pCAGGs-Bcl-XL-IRES-GFP or pCAGGs-empty-IRES-GFP in the presence of growth factors (division conditions). Growth factors were withdrawn 24 h later after transfection, and cells were allowed to differentiate another 7 d (D8). The number of Tuj1$^+$ cells of transfected cells (GFP$^+$ cells) was quantified. (B) Representative images of Tuj1, GFP, and Hoescht IF of hNPCs. (C) Scheme of p53 assay in hNPCs; cell were transfected as in A, cultures were allowed to differentiate for 48 h, and then transfected cells were sorted by means of GFP expression, and lysates were extracted and blotted. (D) Representative Western blot of lysates extracted from 75,000 cells. Membranes were probed against p53, β-actin, and Bcl-XL (three independent experiments). (E) Quantification of p53$^+$ cells on day 2 of differentiation; hNPCs were treated for 10 h with 250 μM ATP. (F). Representative images of p53 and Hoescht IF. Scale bar, 10 mm. (G, I) Number of double Tuj1$^+$/Brdu$^+$ cells from the total number of Tuj1$^+$ cells. Cultures were treated on day 1 of differentiation with 250 mM ATP during 10 h, on day 2 cells were pulsed with 1 μM BrdU for 24 h, and then cells were allowed to differentiate until day 8. (H) Images of IF for Tuj1 and BrdU of control and ATP-treated hNPCs. (I) Quantification of Tuj1$^+$ cells on day 8 of differentiation that were treated with 250 mM ATP for 10 h on day 1. (J) Images of Tuj1 and Hoescht IF. Scale bar, 25 μm. Data represent means ± SEM. Asterisk indicates significant difference ($p < 0.05$, Student's *t* test).

proliferation and differentiation (Salomoni and Calegari, 2010). In this way, we observed an increment in the total cell cycle and S-phase length in the presence of Bcl-XL on day 1 of differentiation (Figure 2D). The recent observations that mouse IPs have a longer cell cycle than apical progenitors and that a prolonged S phase is related to a more proliferative than neurogenic state (Arai *et al.*, 2011) support the assertion that Bcl-XL increases the IP population. Moreover, the data gathered from expression of *Insm1*, *Sox2*, *Pax6*, *Btg2* (Figure 1; Iacopetti *et al.*, 1999; Graham *et al.*, 2003; Englund *et al.*, 2005; Farkas *et al.*, 2008) and the protein levels of the cell cycle inhibitor p27 (Figure 3C), which is up-regulated in the process of differentiative neurogenic divisions (Doetsch *et al.*, 2002; Nguyen *et al.*, 2006), strongly support the model in which Bcl-XL promotes a proliferative state of IPs on the first days of differentiation. This enhanced self-amplifying capacity allows augmentation of the population of IPs. In addition, we found that levels of *Hes5*, a Notch pathway target, are down-regulated on day 3 in the presence of Bcl-XL (unpublished data), supporting the model of a neurogenic population being expanded. At a later time, the neurogenic capacity of the IPs appears, as *Ngn2* expression increases on day 3 of differentiation (Figure 1C; Schuurmans *et al.*, 2004).

Previous experiments proved the cell cycle length hypothesis in relation to neuron generation in mouse NPCs (Calegari and Huttner, 2003), and recent work explained

how cell cycle progression controls the transcriptional activity of Ngn2 (Ali *et al.*, 2011). Now we provide data establishing that the control of cell cycle length is conserved in human NPCs (Figure 2G), and we also demonstrate that changes in cell cycle length influence the decision of an uncommitted NPC to become an IP (Figures 2H and 7D).

Calcium signaling from the ER controls cell cycle length, IPs, and neuron generation

The role of calcium in proliferation as a synchronizing signal for cell cycle is well established in *Xenopus* embryos (Swanson *et al.*, 1997). In CNS development, calcium was proposed as one of the internal cues that control neurogenic timing linked with the cell cycle (Lenos and Tsaniklidou, 2011). Moreover, calcium oscillations have been reported in P19 cells, neurospheres, and the ventricular zone (VZ) of embryonic mice (Scemes *et al.*, 2003; Weissman *et al.*, 2004; Resende *et al.*, 2010). In mouse cortical slices, calcium oscillations are induced by ATP, which triggers the Ins3P receptor–dependent calcium mobilization, leading to the generation of a calcium wave throughout the VZ. The number of cells responding to the signal and the intensity and propagation of the wave increase during the neurogenic period. The result of this calcium wave is a higher progenitor proliferation (Weissman *et al.*, 2004).

Bcl-XL modulates the sensitivity of the inositol trisphosphate (inositol 1,4,5-trisphosphate; InsP3) receptor by direct binding, causing a higher activity under subsaturating concentrations of the receptor agonists. In addition, Bcl-XL enhances the spontaneous calcium release by Ins3P (White *et al.*, 2005; Li *et al.*, 2007). This Bcl-XL relationship with calcium led us to believe that Bcl-XL could modulate IP proliferation and, as a consequence, final neuronal output, by modulation of cytosolic calcium (Figure 5). In agreement with this model, we first determined that Bcl-XL cells had higher cytosolic calcium levels than control cells on day 1 (Figure 5B). Second, the addition of calcium chelators blocked the effect of Bcl-XL on neurogenesis (Figure 5, D and E). Third, the manipulation of Bcl-XL levels tunes the neurogenic ATP-evoked response (Figure 6, D and E, and Supplemental Figure S5). Other proteins of the Bcl-2 family—Bax and Bak—have been reported to alter T cell progenitor proliferation by modulating ER calcium signaling, supporting the view that Bcl-2 proteins could regulate proliferation under physiological conditions by means of their ability to control calcium dynamics (Jones *et al.*, 2007; Lamb and Hardwick, 2010).

Several studies showed that an increase in cytosolic calcium in response to different stimuli, such as ATP, acetylcholine, γ-aminobutyric acid, or glutamate, produces an increase of proliferation and, in some models, an increase in differentiation (Haydar *et al.*, 2000; Ryu *et al.*, 2003; Resende *et al.*, 2008a, 2008b). We intended to extend our findings of calcium-mediated control of the cell cycle length and thus of IP and neuron generation. We demonstrated that the effect observed with manipulation of Bcl-XL could be also induced by Tg-promoted calcium release (Figure 5K) and by ATP-evoked calcium mobilization through the Ins3P pathway (Figures 5, I, J, and L; 7, A–C; and 9, E–J). Hence, the presented data contribute to an understanding of how calcium mobilization, evoked by different means, is able to modulate cell cycle length, IP proliferation, and neuron generation.

Calcium mobilization controls neurogenesis through p53 levels

Among the cell cycle regulators, p21 was the only member whose expression was increased in the presence of elevated Bcl-XL on day 1 (Figure 3A). The tumor suppressor p53, a transcriptional regulator of p21, was increased in Bcl-XL cells (Figures 3, D and E; 4, A and B; and 9D). Furthermore, we demonstrated that decreased p53 levels prevent the neurogenic effect of Bcl-XL and ATP on hNPC differentiation (Figures 4, E and F, and 8E). Several studies demonstrated that p53 is involved in other events during neural development and not just in the cell death/survival decision (Tedeschi and Di Giovanni, 2009). For instance, p53 has been reported to regulate the neuronal outcome by inhibiting Id1 expression in NPCs. This protein is an inhibitor of bHLH transcription factors, such as Ngn2. Thus this function of p53 may explain the increase in Ngn2 observed on day 3 in our system (Aranha *et al.*, 2009).

Calcium can modulate the cell cycle by several pathways (Martins and Pearson, 2008). Indeed, some of them control p53 expression, that is, an increase in calcium transient signals enhances the phosphorylation of cAMP-responsive element-binding protein (CREB) by calmodulin kinase or mitogen-activated protein kinase and promotes CREB-binding protein/p300 activity and p53 transactivation. This p53 activation promotes p21 expression, which results in growth arrest (Chrivia *et al.*, 1993; Arias *et al.*, 1994; Arnould *et al.*, 2002). However, we propose a model in which periodic calcium release from the ER elevates mitochondrial matrix calcium and regulates mitochondrial bioenergetics (White *et al.*, 2005; Li *et al.*, 2007). Mitochondrial signals have been proposed as a mechanism used to synchronize the cell cycle during morphogenesis of the eye imaginal disk in *Drosophila*. In this model, the genetic modification of a subunit of mitochondrial electron-transport complex IV produces lower amounts of ATP and triggers p53 phosphorylation by AMP-activated protein kinase, causing the cells to arrest in G1/S checkpoint, synchronizing the cells for their last division before differentiating (Mandal *et al.*, 2005; Owusu-Ansah *et al.*, 2008). First, we favor this pathway based on preliminary data showing that extracellular signal-regulated kinase phosphorylation is altered after ATP treatment but its inhibition does not affect p53 levels (unpublished data). Second, Bcl-XL has a mitochondrial pattern localization, meaning that it may be localized at ER–mitochondrial microdomains. (Figure 4G). Third, Bcl-XL alters mitochondrial bioenergetics and modulates intracellular levels of ATP (Alavian *et al.*, 2011). Finally, promyelocytic leukemia–another protein implicated in the communication between ER and mitochondria through the InsP3 receptor—is involved in the proliferation versus differentiation decision in mouse cortex development (Regad *et al.*, 2009; Giorgi *et al.*, 2010).

Overall, the presented data help to understand how cell cycle length can control the mode of NPC division during neurogenesis and how calcium, as an upstream signal, controls the cell cycle. The decision between proliferation and differentiation is crucial during development, and it is also important for neurodegenerative diseases in which aberrant cell cycle reentry is observed or in conditions of uncontrolled proliferation, as in cancer. Advances in the knowledge of these processes may help to develop future therapies.

MATERIALS AND METHODS

Cell culture of immortalized and nonimmortalized human neural progenitors/stem cells

In this study we used control hNS1 cells, primary human neural progenitors, and their counterparts after the forced expression of Bcl-XL. The hNS1 cell line is a v-myc immortalized, nontransformed, human fetal forebrain–derived, multipotent, clonal cell line of neural stem cells (Villa *et al.*, 2000). hNS1 cell culture conditions are based on a chemically defined HSC medium that consists of DMEM/F12 (Life Technologies, Carlsbad, CA) supplemented with N2 supplement (100X; Life Technologies), 6 g/l glucose (Sigma-Aldrich, St. Louis, MO), 0.5% AlbuMAX-I (Life Technologies), 5 mM

4-(2-hydroxyethyl)-1-piperazineethanesulfonic acid (HEPES; Life Technologies), and nonessential amino acids. Proliferation conditions were achieved by supplementing HSC medium with 20 ng/ml of each recombinant human epidermal growth factor (EGF) and basic fibroblast growth factor (FGF2; R&D Systems, Minneapolis, MN), and differentiation conditions were obtained after mitogen withdrawal (EGF, FGF2). Cells were grown at 5% CO_2 and normal atmospheric oxygen levels (20% O_2). To perform an experiment, cells were seeded at 25,000 cell/cm^2 (unless otherwise indicated) on poly-L-lysine (10 µg/ml; Sigma-Aldrich)–coated plastic or poly-L-lysine (25–50 µg/ml) glass coverslips with HSC medium containing EGF and FGF2. After 24 h, growth factors were withdrawn and the cultures were allowed to differentiate, with a change of two-thirds of the medium every second day. The generation of Bcl-XL–overexpressing cells (hNS1 subclone 3) was previously described (Liste *et al.*, 2004); these Bcl-XL cells grow and differentiate in the same conditions as hNS1.

Primary human neural progenitors were obtained from tissue of an aborted human fetus of 9.5 wk gestational age (Bengt Juliusson, Lund University Hospital/Wallenberg Neuroscience Center, Lund, Sweden). The tissue was donated for research after informed consent and following European Union directives, Network of European CNS Transplantation and Regeneration recommendations, and Spanish laws RD 42/1988 and 14/2007. All procedures followed Society for Neuroscience recommendations and were also approved by the Bioethics of Research Committee of the Autonomous University of Madrid (Spain). These primary progenitors grow as a neurosphere culture in HSC medium supplemented with EGF and FGF2, 20 ng/ml, and subcultured by mechanical protocols. When used for experimentation, cells were seeded as adherent cultures (1×10^5 cell/cm^2 unless otherwise indicated) on plastic or glass coverslips coated with 50 µg/ml poly-L-lysine and 1 µg/ml laminin in proliferation conditions. After 24 h, growth factors were withdrawn and hNPCs were differentiated for the indicated times.

In some experiments, control and Bcl-XL hNS1 cells were treated with 10 µM oloumicine or 10 µM iso-oloumicine during 24 h to slow the cell cycle progression. To modify cytosolic calcium, cells were treated with 0.7 µM ethylene glycol tetraacetic acid (EGTA) and 10 µM BAPTA-AM or 250µM ATP for 24 h on day 1 of differentiation (reduction or increase in Ca_i, respectively).

Vectors, transfection, and viral infection

Bcl-XL was cloned by real-time PCR, using random primers, from human cDNA obtained from hNS1 cells with the following primers: 5′-TTGGACAATGGACTGGTTGA-3′ and 5′-gggagggtagagtggatggt-3′. The amplified product was cloned into the pST1blue vector by Perfectly Blunt Cloning Kit (Novagen, EMD4Biosciences, Gibbstown, NJ) following the manufacturer's instructions. Next Bcl-XL was subcloned into pCAAGS-NLS-IRES-GFP expression vector (a gift from F. Guillemot's laboratory, National Institute for Medical Research, London, United Kingdom) by pST1blue-Bcl-XL digestion with *Mlu*I and *Sac*I enzymes. The fusion cDNA encoding FLAG-Bcl-XL used for colocalization studies was generated from pST-1blue-Bcl-XL vector by PCR with 5′-CTGCCACCATGGACTACAAAGACGATGACGACAAGATGTCTCAGAGCAACCGGG-3′ and 5′-gggagggtagagtggatggt-3′ pair primer. Then it was subcloned into pCAAGS-NLS-IRES-GFP vector by *Mlu*I/*Nhe*I digestion.

Validated p53 shRNA sequences were purchased cloned into pLKO.1-cytomegalovirus (CMV)-tGFP (Sigma-Aldrich). The sequences were as follows: shRNA 14, CCGGGAGGGATGTTTGGGAGATGTACTCGAGTACATCTCCCAAACATCCCTCTTTTT; shRNA 53, CCGGCGGCGCACAGAGGAAGAGAATCTCGAGATTCTCTTCCTCTGTGCGCCGTTTTT; shRNA 54, CCGGTCAGACCTATGGAAACTACTTCTCGAGAAGTAGTTTCCATAGGTCTGATTTTT; shRNA 55, CCGGGTCCAGATGAAGCTCCCAGAACTCGAGTTCTGGGAGCTTCATCTGGACTTTTT;and shRNA 56, CCGGCACCATCCACTACAACTACATCTCGAGATGTAGTTGTAGTGGATGGTGTTTTT.

The two controls used were pLKO.1 nontarget shRNA-puro vector (shRNA control), whose shRNA does not target any known human gene but will engage with RISC and a pLKO.1-puro CMV-tGFP-control vector that contains a gene encoding tGFP driven by the CMV promoter.

Viral packaging was achieved by cotransfecting every pLKO.1-shRNA-CMV-tGFP vector with pCMVdR and pMD2G packaging vectors (Sigma-Aldrich) with Lipofectamine2000 (Invitrogen, Carlsbad, CA) into 293T cells following the manufacturer's instructions. 293T cells used to pack lentivirus were grown in DMEM, glutamine, and 5% fetal bovine serum at 5% CO_2 and normal atmospheric oxygen levels (20% O_2).

Viral particles were collected in HSC medium. Titers were determined on hNS1 cells, resulting in ~4×10^5 transducing units/ml for every shRNA vector, and lentiviral particles were used to infect at a multiple of infection (MOI) of 2 particles/cell. Infected cells were detected by the expression of tGFP.

For human and rat Bcl-XL shRNA cloned into pLKO.1-puro vector, lentiviral particles were purchased from Sigma-Aldrich. They were used at MOI of 1. Infection efficiency was quantified after 48 h of exposure of infected cultures to 1 mg/ml puromycin. The sequences were as follows: shRNA 99, CCGGGCTCACTCTTCAGTCGGAAATCTCGAGATTTCCGACTGAAGAGTGAGCTTTTT;G; shRNA 00, CCGGGTGGAACTCTATGGGAACAATCTCGAGATTGTTCCCATAGAGTTCCACTTTTT;G; shRNA 01, CCGGGTTTAGTGATGTGGAAGAGAACTCGAGTTCTCTTCCACATCACTAAACTTTTT; G; shRNA 02, CCGGAGAGCTTTGAACAGGATACTTCTCGAGAAGTATCCTGTTCAAAGCTCTTTTTT;G; shRNA 03, CCGGCGACGAGTTTGAACTGCGGTACTCGAGTACCGCAGTTCAAACTCGTCGTTTTT;G; shRNA 05, CCGGCGATGAGTTTGAACTGCGGTACTCGAGTACCGCAGTTCAAACTCATCGTTTTT; shRNA83, CCGGGTGGATCTCTACGGGAACAATCTCGAGATTGTTCCCGTAGAGATCCACTTTTT; and shRNA84, CCGGCAGGTATTGGTGAGTCGGATTCTCGAGAATCCGACTCACCAATACCTGTTTTT.

RNA extraction and quantitative real-time PCR

Cells were trypsinized, washed, and distributed in aliquots of two to three million cells. RNA was extracted with High Pure RNA Isolation kit (Roche, Indianapolis, IN) following the manufacturer's instructions. RNA purity and concentration were measured in a NanoDrop (Thermo Scientific, Wilmington, DE). Next 1 µg of RNA was retrotranscripted with a High-Capacity cDNA Archive Kit (Applied Biosystems, Foster City, CA). Reverse transcription reaction settings were 10 min at 25°C and 2 h at 37°C and 4°C.

Real-time PCR was performed to relatively quantify mRNA expression using TaqMan probes (Applied Biosystems) *Sox2*, Hs01053049_s1; *Pax6*, Hs00240871_m1; *Ngn2*, Hs00702774_s1; *NeuroD1*, Hs00159598_m1; *Btg2*, Hs019887_m1, and *Insm1*, Hs00357871_s1; using the ABI PRISM 7900 HT and 7000 systems (Applied Biosystems). The PCR mixture contained 1 µl of cDNA (0.5 µg/µl) in 8 µl of RNase-free water, 10 µl of TaqMan universal PCR Master Mix, no AmpErase, 2×, and 1 µl of TaqMan probe. The method to quantify the relative fluorescence emission used $2^{-\Delta\Delta Ct}$, where Ct is the cycle when a given reaction reaches a threshold, ΔCt is the normalization by the amount of total RNA, performed with glyceraldehyde-3-phosphate dehydrogenase cDNA, and ΔΔCt is

calculated as the ratio between Bcl-XL and control hNS1 cell ΔCt of a given gene on the separate indicated days.

Analysis of cell cycle length

The experiment is based on the linear incorporation of a thymidine analogue (5-ethynyl-2′-deoxyuridine; EdU) in a uniformly cycling population of cells constantly exposed to it (Nowakowski *et al.*, 1989). In this model, labeled cells just after the initial exposure to EdU would be the time that S phase takes (Ts), so then the fraction of proliferating population (identified as Ki-67$^+$) labeled with EdU (label index) at time 0 is Ts/Tc, where Tc is the time of the total cell cycle. During the experiment, cells linearly incorporate EdU until they reach a maximum labeling index (LI; value, 1) when all of them have already passed once through the S phase and completed one cell cycle. Implicitly, LI = 1 means Tc − Ts. Then, by linear regression ($y = mx + n$), one can obtain Tc and Ts as follows: when $y = 1$, $x = Tc - Ts$, and when $y = 0$, $x = Ts$. To avoid violating the uniformly cycling premise, essential for the validity of the method, we chose to quantify only the Ki67$^+$ cells on day 1 of differentiation, when the cell population is homogeneous.

To perform the experiment, cells were seeded at 25,000 cells/cm^2 on 30 μg/ml poly-L-lysine–coated glass coverslips in proliferation medium. After 24 h, the growth factors were withdrawn. After another 24 h, cells were incubated with 10 μM EdU and fixed at 30 min and then every hour until a total of 6 h. For EdU detection, we used the Click-ITTM EdU Alexa Fluor High-Throughput Imaging (HSC) Assay (Invitrogen). Prior to first antibody incubation, fixed cells were incubated with the solutions supplied by the kit.

Immunofluorescence and immunoblotting

At the specified time points, the cultures were rinsed with 0.1 M phosphate-buffered saline (PBS) and fixed for 15 min in freshly prepared 4% paraformaldehyde (PFA)/piperazine-*N*,*N*′-bis[2-ethane-sulfonic acid] (PIPES), HEPES, EGTA, $MgCl_2$ (PHEM) buffer/4% sucrose. Samples were blocked for 1 h in 10% goat serum and 0.25% Triton X-100 in PBS and incubated overnight at 4°C with mouse monoclonal antibodies against Tuj1 (1:1000; Sigma-Aldrich), p53 (DO1; 1:2000; Santa Cruz Biotechnology, Santa Cruz, CA), and FLAG M2 (1:1000; Sigma-Aldrich) or with rabbit polyclonal antibodies against p53 (1:500; Santa Cruz Biotechnology), GFP (1:500; Invitrogen), rat monoclonal antibody against BrdU (1:1000; Sigma-Aldrich), or rabbit monoclonal antibody against Ki67 (1:2000; Lab Vision, Thermo Scientific, Fremont, CA) dissolved in 1% goat serum and 0.25% Triton X-100 in PBS. On the next day, samples were incubated with goat anti–mouse Cy3–conjugated (1:500; Jackson ImmunoResearch Laboratories, West Grove, PA), goat anti–rabbit A488–conjugated (1:500; Invitrogen), goat anti–rabbit A555–conjugated (1:500; Invitrogen), donkey anti–mouse Cy5–conjugated (1:500; Jackson ImmunoResearch), or goat anti–rat fluorescein isothiocyanate–conjugated (1:500; Jackson ImmunoResearch) antibodies. Cell nuclei were counterstained with Hoescht 33258 (Molecular Probes, Invitrogen) at 0.2 mg/ml in PBS.

For BrdU IF, prior to incubation with the first antibody, fixed cultures were treated with 2 M HCl at 37°C for 30 min, followed by three rinses in 0.1 M borate buffer (pH 8.9). For double immunofluorescence (IF; BrdU and other antigens), BrdU processing and staining was performed as a second IF round.

For nuclear extracts, cultures were lysed in ice-cold buffer (15 mM HEPES, 10 mM KCl, 2 mM MgCl, 250 mM sucrose, 50 mM dithiothreitol, 10% glycerol, digitonin 0.05%, and phosphate and protease inhibitor cocktail tablet [Roche]) for 5 min and then homogenized with 10 strokes in a loose-fitting Dounce. The lysate was spun at 3000 × *g* for 5 min at 4°C, and the supernatant-cytosolic fraction was discarded and the pellet was resuspended in the same buffer without digitonin. For Western blotting, 30–50 μg of protein was loaded into a 10–12% polyacrylamide gel, electrophoresed, and transferred to a nitrocellulose membrane. Membranes were blocked with 5% skimmed milk and 0.05% Tween 20 in 50 mM Tris-buffered saline. Then membranes were incubated at 4°C overnight with mouse monoclonal antibodies against p57 (1:200; BD Transduction Laboratories, Lexington, KY), p27 (1:5000; BD Transduction Laboratories), p21 (1:1000; BD Biosciences PharMingen, San Diego, CA), p53 (DO1; 1:2000, Santa Cruz Biotechnology), β-actin (1:5000; Sigma-Aldrich), and lamin A + C (1:500; Abcam, Cambridge, MA) or rabbit polyclonal antibodies against Bcl-XL (1:500; BD Transduction Laboratories) in 1% skimmed milk and 0.05% Tween 20 in 50 mM TBS. Secondary antibodies were tagged with horseradish peroxidase and were horse anti-mouse peroxidase (1:10,000; Vector Laboratories, Burlingame, CA) and goat anti–rabbit peroxidase (1:5000; Nordic Immunology, Tilburg, Netherlands) The blots were developed using the ECL System (Amersham-Pharmacia Biotech, GE Healthcare Bio-Sciences, Piscataway, NJ).

Fluorescence-activated cell sorting

Cells were collected on day 1 of differentiation in a buffer containing 5 mM EDTA and 25 mM HEPES in PBS at 3×10^6 cell/ml. Cells were excited with a 488-nm laser and sorted by means of GFP expression with an FL2 fluorescence detector using a FACSVantage sorter (BD Biosciences, Sparks, MD).

Measurement of cytosolic free calcium

For bulk experiments the cells were seeded at 50,000 cells/cm^2 on 10 μg/ml poly-L-lysine–coated 24-well plates. On chosen days (DIV, days 1 and 3), the medium was discarded and cells were incubated with 5 μM Fura2-AM in 120 mM NaCl, 5.4 mM KCl, 0.8 mM $MgCl_2$, 20 mM HEPES, 10 mM NaOH, and 2 mM glucose, pH 7.4, per well, during 30 min at 37°C. After loading, the cells were washed with Hank's balanced salt solution with 2 mM $CaCl_2$ and incubated for an additional 30 min at 37°C. The Fura2 signal was gathered ratiometrically using alternate excitation at 340 and 380 nm and a 510-nm emission filter with FLUOstar OPTIMA (BMG Labtech, Ortenberg, Germany).

For single-cell calcium imaging, cells were seeded at 20,000 cells/cm^2 on 10 μg/ml poly-L-lysine–coated 24-well plates on day 1 of differentiation, the medium was discarded, and cells were incubated with 5 μM Fura2-AM in 120 mM NaCl, 5.4 mM KCl, 0.8 mM $MgCl_2$, 20 mM HEPES, 10 mM NaOH, and 2 mM glucose, pH 7.4, per well during 30 min at 37°C. After loading, the cells were washed with HBBS with 2 mM $CaCl_2$ and incubated for an additional 30 min at 37°C. The coverslips were mounted in a chamber on the microscope stage as described earlier (Martinez-Serrano *et al.*, 1996) and Fura-2 fluorescence was imaged ratiometrically using alternate excitation at 340 and 380 nm and a 510-nm emission filter with a Neofluar 40×/0.75 objective (Carl Zeiss, Jena, Germany) at 37°C. Additions as indicated were made as a bolus. Single-cell analysis of the changes in $[Ca^{2+}]_i$ were expressed as the ratio of fluorescence intensity at 340 (F_{340}) and 380 nm (F_{380}; F_{340}/F_{380}). Image acquisition and analysis were performed with Aquacosmos 2.5 software (Hamamatsu, Hamamatsu, Japan).

Image and data analyses

Analyses and photography of fluorescent cultures were done in an inverted Axiovert 135 microscope (Carl Zeiss) equipped with a Leica DFC345FX digital camera (Leica, Wetzlar, Germany). Image

analyses were performed using ImageJ software. Confocal images were taken with LSM510 META (Carl Zeiss). Orthogonal projections from images were performed with LSM Image Browser software. Statistical tests were run using Statistica, version 7, software. Results are shown as the average ± SEM of data from three to five experiments, unless stated otherwise.

ACKNOWLEDGMENTS

We thank Milagros Ramos, Jorgina Satrústegui, and members of the Satrústegui laboratory (Centro de Biología Molecular "Severo Ochoa" [CBMSO], Madrid, Spain) for calcium imaging assistance, Isabel Liste (CBMSO) for fruitful discussions, Bengt Juliusson (Lund University Hospital, Lund, Sweden) for providing human neurospheres, and François Guillemot (National Institute for Medical Research) for sharing a modified pCAGGs vector. We thank Jon Gil and Héctor Díez (CBMSO) for help with lentiviral vector packaging. We are also grateful to Ricardo Ramos (Scientific Park, Madrid) for quantitative real-time PCR determinations and Berta Raposo and Veronica Labrador for cytometry and confocal microscopy assistance. The excellent technical assistance of Beatriz Moreno and Ignacio Tardieu is also gratefully acknowledged. This work was supported by European Union Grant NMP-SL-2008-214706 EXCELL, Spanish Ministry of Science and Technology Grant SAF2004-03405, Spanish Ministry of Science and Innovation Grants BIO2007-66807, PLE2009-0101, and SAF2010-17167, Carlos III Institute of Health Grant RETICS TerCel RD06/0010/0009, and La Caixa Foundation Grant BM05-22-0). This work was also supported by an institutional grant from Foundation Ramón Areces to the Center of Molecular Biology "Severo Ochoa."

REFERENCES

Alavian KN *et al.* (2011). Bcl-xL regulates metabolic efficiency of neurons through interaction with the mitochondrial F1FO ATP synthase. Nat Cell Biol 13, 1224–1233.

Ali F, Hindley C, McDowell G, Deibler R, Jones A, Kirschner M, Guillemot F, Philpott A (2011). Cell cycle-regulated multi-site phosphorylation of Neurogenin 2 coordinates cell cycling with differentiation during neurogenesis. Development 138, 4267–4277.

Arai Y, Pulvers JN, Haffner C, Schilling B, Nusslein I, Calegari F, Huttner WB (2011). Neural stem and progenitor cells shorten S-phase on commitment to neuron production. Nat Commun 2, 154.

Aranha MM, Sola S, Low WC, Steer CJ, Rodrigues CM (2009). Caspases and p53 modulate FOXO3A/Id1 signaling during mouse neural stem cell differentiation. J Cell Biochem 107, 748–758.

Arias J, Alberts AS, Brindle P, Claret FX, Smeal T, Karin M, Feramisco J, Montminy M (1994). Activation of cAMP and mitogen responsive genes relies on a common nuclear factor. Nature 370, 226–229.

Arnould T, Vankoningsloo S, Renard P, Houbion A, Ninane N, Demazy C, Remacle J, Raes M (2002). CREB activation induced by mitochondrial dysfunction is a new signaling pathway that impairs cell proliferation. EMBO J 21, 53–63.

Besson A, Dowdy SF, Roberts JM (2008). CDK inhibitors: cell cycle regulators and beyond. Dev Cell 14, 159–169.

Bond J, Woods CG (2006). Cytoskeletal genes regulating brain size. Curr Opin Cell Biol 18, 95–101.

Boulaire J, Fotedar A, Fotedar R (2000). The functions of the cdk-cyclin kinase inhibitor p21WAF1. Pathol Biol (Paris) 48, 190–202.

Calegari F, Huttner WB (2003). An inhibition of cyclin-dependent kinases that lengthens, but does not arrest, neuroepithelial cell cycle induces premature neurogenesis. J Cell Sci 116, 4947–4955.

Chang MY *et al.* (2007). Bcl-XL/Bax proteins direct the fate of embryonic cortical precursor cells. Mol Cell Biol 27, 4293–4305.

Chrivia JC, Kwok RP, Lamb N, Hagiwara M, Montminy MR, Goodman RH (1993). Phosphorylated CREB binds specifically to the nuclear protein CBP. Nature 365, 855–859.

Courtois ET, Castillo CG, Seiz EG, Ramos M, Bueno C, Liste I, Martinez-Serrano A (2010). In vitro and in vivo enhanced generation of human A9 dopamine neurons from neural stem cells by Bcl-XL. J Biol Chem 285, 9881–9897.

Dehay C, Kennedy H (2007). Cell-cycle control and cortical development. Nat Rev Neurosci 8, 438–450.

Doe CQ (2008). Neural stem cells: balancing self-renewal with differentiation. Development 135, 1575–1587.

Doetsch F, Verdugo JM, Caille I, Alvarez-Buylla A, Chao MV, Casaccia-Bonnefil P (2002). Lack of the cell-cycle inhibitor p27Kip1 results in selective increase of transit-amplifying cells for adult neurogenesis. J Neurosci 22, 2255–2264.

Englund C, Fink A, Lau C, Pham D, Daza RA, Bulfone A, Kowalczyk T, Hevner RF (2005). Pax6, Tbr2, and Tbr1 are expressed sequentially by radial glia, intermediate progenitor cells, and postmitotic neurons in developing neocortex. J Neurosci 25, 247–251.

Farkas LM, Haffner C, Giger T, Khaitovich P, Nowick K, Birchmeier C, Paabo S, Huttner WB (2008). Insulinoma-associated 1 has a panneurogenic role and promotes the generation and expansion of basal progenitors in the developing mouse neocortex. Neuron 60, 40–55.

Farkas LM, Huttner WB (2008). The cell biology of neural stem and progenitor cells and its significance for their proliferation versus differentiation during mammalian brain development. Curr Opin Cell Biol 20, 707–715.

Fish JL, Dehay C, Kennedy H, Huttner WB (2008). Making bigger brains—the evolution of neural-progenitor-cell division. J Cell Sci 121, 2783–2793.

Garrido C, Kroemer G (2004). Life's smile, death's grin: vital functions of apoptosis-executing proteins. Curr Opin Cell Biol 16, 639–646.

Giorgi C *et al.* (2010). PML regulates apoptosis at endoplasmic reticulum by modulating calcium release. Science 330, 1247–1251.

Gotz M, Huttner WB (2005). The cell biology of neurogenesis. Nat Rev Mol Cell Biol 6, 777–788.

Graham V, Khudyakov J, Ellis P, Pevny L (2003). SOX2 functions to maintain neural progenitor identity. Neuron 39, 749–765.

Guillemot F (2007). Cell fate specification in the mammalian telencephalon. Prog Neurobiol 83, 37–52.

Hagn F, Klein C, Demmer O, Marchenko N, Vaseva A, Moll UM, Kessler H (2010). BclxL changes conformation upon binding to wild-type but not mutant p53 DNA binding domain. J Biol Chem 285, 3439–3450.

Haydar TF, Wang F, Schwartz ML, Rakic P (2000). Differential modulation of proliferation in the neocortical ventricular and subventricular zones. J Neurosci 20, 5764–5774.

Huttner WB, Kosodo Y (2005). Symmetric versus asymmetric cell division during neurogenesis in the developing vertebrate central nervous system. Curr Opin Cell Biol 17, 648–657.

Iacopetti P, Michelini M, Stuckmann I, Oback B, Aaku-Saraste E, Huttner WB (1999). Expression of the antiproliferative gene TIS21 at the onset of neurogenesis identifies single neuroepithelial cells that switch from proliferative to neuron-generating division. Proc Natl Acad Sci USA 96, 4639–4644.

Janumyan Y, Cui Q, Yan L, Sansam CG, Valentin M, Yang E (2008). G0 function of BCL2 and BCL-xL requires BAX, BAK, and p27 phosphorylation by Mirk, revealing a novel role of BAX and BAK in quiescence regulation. J Biol Chem 283, 34108–34120.

Jones RG *et al.* (2007). The proapoptotic factors Bax and Bak regulate T Cell proliferation through control of endoplasmic reticulum Ca(2+) homeostasis. Immunity 27, 268–280.

Joseph B, Hermanson O (2010). Molecular control of brain size: regulators of neural stem cell life, death and beyond. Exp Cell Res 316, 1415–1421.

Kriegstein A, Noctor S, Martinez-Cerdeno V (2006). Patterns of neural stem and progenitor cell division may underlie evolutionary cortical expansion. Nat Rev Neurosci 7, 883–890.

Kuranaga E (2011). Caspase signaling in animal development. Dev Growth Differ 53, 137–148.

Kuranaga E, Miura M (2007). Nonapoptotic functions of caspases: caspases as regulatory molecules for immunity and cell-fate determination. Trends Cell Biol 17, 135–144.

Lamb HM, Hardwick M (2010). Noncanonical functions of BCL-2 proteins in the nervous system. Adv Exp Med Biol 687, 115–129.

Lenos MG, Tsaniklidou SM (2010). Calcium oscillations, G1 phase duration and neurogenesis timing. Trends Cell Biol 20, 577; author reply 578.

Li C, Wang X, Vais H, Thompson CB, Foskett JK, White C (2007). Apoptosis regulation by Bcl-x(L) modulation of mammalian inositol 1,4,5-trisphosphate receptor channel isoform gating. Proc Natl Acad Sci USA 104, 12565–12570.

Lindsten T, Golden JA, Zong WX, Minarcik J, Harris MH, Thompson CB (2003). The proapoptotic activities of Bax and Bak limit the size of the neural stem cell pool. J Neurosci 23, 11112–11119.
Lipskaia L, Hulot JS, Lompre AM (2009). Role of sarco/endoplasmic reticulum calcium content and calcium ATPase activity in the control of cell growth and proliferation. Pflugers Arch 457, 673–685.
Liste I, Garcia-Garcia E, Bueno C, Martinez-Serrano A (2007). Bcl-XL modulates the differentiation of immortalized human neural stem cells. Cell Death Differ 14, 1880–1892.
Liste I, Garcia-Garcia E, Martinez-Serrano A (2004). The generation of dopaminergic neurons by human neural stem cells is enhanced by Bcl-XL, both in vitro and in vivo. J Neurosci 24, 10786–10795.
Mandal S, Guptan P, Owusu-Ansah E, Banerjee U (2005). Mitochondrial regulation of cell cycle progression during development as revealed by the tenured mutation in *Drosophila*. Dev Cell 9, 843–854.
Martins RA, Pearson RA (2008). Control of cell proliferation by neurotransmitters in the developing vertebrate retina. Brain Res 4, 119237–60.
Martinez-Serrano A, Borner C, Pereira R, Villalba M, Satrustegui J (1996). Modulation of presynaptic calcium homeostasis by nitric oxide. Cell Calcium 20, 293–302.
Miyata T, Kawaguchi A, Saito K, Kawano M, Muto T, Ogawa M (2004). Asymmetric production of surface-dividing and non-surface-dividing cortical progenitor cells. Development 131, 3133–3145.
Nguyen L, Besson A, Roberts JM, Guillemot F (2006). Coupling cell cycle exit, neuronal differentiation and migration in cortical neurogenesis. Cell Cycle 5, 2314–2318.
Noctor SC, Martinez-Cerdeno V, Kriegstein AR (2008). Distinct behaviors of neural stem and progenitor cells underlie cortical neurogenesis. J Comp Neurol 508, 28–44.
Nowakowski RS, Lewin SB, Miller MW (1989). Bromodeoxyuridine immunohistochemical determination of the lengths of the cell cycle and the DNA-synthetic phase for an anatomically defined population. J Neurocytol 18, 311–318.
Ohnuma S, Philpott A, Harris WA (2001). Cell cycle and cell fate in the nervous system. Curr Opin Neurobiol 11, 66–73.
Owusu-Ansah E, Yavari A, Mandal S, Banerjee U (2008). Distinct mitochondrial retrograde signals control the G1-S cell cycle checkpoint. Nat Genet 40, 356–361.
Qian X, Shen Q, Goderie SK, He W, Capela A, Davis AA, Temple S (2000). Timing of CNS cell generation: a programmed sequence of neuron and glial cell production from isolated murine cortical stem cells. Neuron 28, 69–80.
Regad T, Bellodi C, Nicotera P, Salomoni P (2009). The tumor suppressor Pml regulates cell fate in the developing neocortex. Nat Neurosci 12, 132–140.
Resende RR, Adhikari A, da Costa JL, Lorencon E, Ladeira MS, Guatimosim S, Kihara AH, Ladeira LO (2010). Influence of spontaneous calcium events on cell-cycle progression in embryonal carcinoma and adult stem cells. Biochim Biophys Acta 1803, 246–260.
Resende RR, Britto LR, Ulrich H (2008a). Pharmacological properties of purinergic receptors and their effects on proliferation and induction of neuronal differentiation of P19 embryonal carcinoma cells. Int J Dev Neurosci 26, 763–777.
Resende RR, Gomes KN, Adhikari A, Britto LR, Ulrich H (2008b). Mechanism of acetylcholine-induced calcium signaling during neuronal differentiation of P19 embryonal carcinoma cells in vitro. Cell Calcium 43, 107–121.
Ryu JK, Choi HB, Hatori K, Heisel RL, Pelech SL, McLarnon JG, Kim SU (2003). Adenosine triphosphate induces proliferation of human neural stem cells: Role of calcium and p70 ribosomal protein S6 kinase. J Neurosci Res 72, 352–362.
Salomoni P, Calegari F (2010). Cell cycle control of mammalian neural stem cells: putting a speed limit on G1. Trends Cell Biol 20, 233–243.
Scemes E, Duval N, Meda P (2003). Reduced expression of P2Y1 receptors in connexin43-null mice alters calcium signaling and migration of neural progenitor cells. J Neurosci 23, 11444–11452.
Schuurmans C *et al.* (2004). Sequential phases of cortical specification involve Neurogenin-dependent and -independent pathways. EMBO J 23, 2892–2902.
Shen Q, Wang Y, Dimos JT, Fasano CA, Phoenix TN, Lemischka IR, Ivanova NB, Stifani S, Morrisey EE, Temple S (2006). The timing of cortical neurogenesis is encoded within lineages of individual progenitor cells. Nat Neurosci 9, 743–751.
Shim JW, Koh HC, Chang MY, Roh E, Choi CY, Oh YJ, Son H, Lee YS, Studer L, Lee SH (2004). Enhanced in vitro midbrain dopamine neuron differentiation, dopaminergic function, neurite outgrowth, and 1-methyl-4-phenylpyridium resistance in mouse embryonic stem cells overexpressing Bcl-XL. J Neurosci 24, 843–852.
Swanson CA, Arkin AP, Ross J (1997). An endogenous calcium oscillator may control early embryonic division. Proc Natl Acad Sci USA 94, 1194–1199.
Tedeschi A, Di Giovanni S (2009). The non-apoptotic role of p53 in neuronal biology: enlightening the dark side of the moon. EMBO Rep 10, 576–583.
Villa A, Snyder EY, Vescovi A, Martinez-Serrano A (2000). Establishment and properties of a growth factor-dependent, perpetual neural stem cell line from the human CNS. Exp Neurol 161, 67–84.
Weissman TA, Riquelme PA, Ivic L, Flint AC, Kriegstein AR (2004). Calcium waves propagate through radial glial cells and modulate proliferation in the developing neocortex. Neuron 43, 647–661.
White C, Li C, Yang J, Petrenko NB, Madesh M, Thompson CB, Foskett JK (2005). The endoplasmic reticulum gateway to apoptosis by Bcl-X(L) modulation of the InsP3R. Nat Cell Biol 7, 1021–1028.
Youle RJ, Strasser A (2008). The BCL-2 protein family: opposing activities that mediate cell death. Nat Rev Mol Cell Biol 9, 47–59.
Zhong W, Chia W (2008). Neurogenesis and asymmetric cell division. Curr Opin Neurobiol 18, 4–11.
Zinkel S, Gross A, Yang E (2006). BCL2 family in DNA damage and cell cycle control. Cell Death Differ 13, 1351–1359.